Okinawa Institute of Science and Technology
Graduate University

Thesis submitted for the degree

Doctor of Philosophy

Advanced split-operator techniques for simulating quantum systems

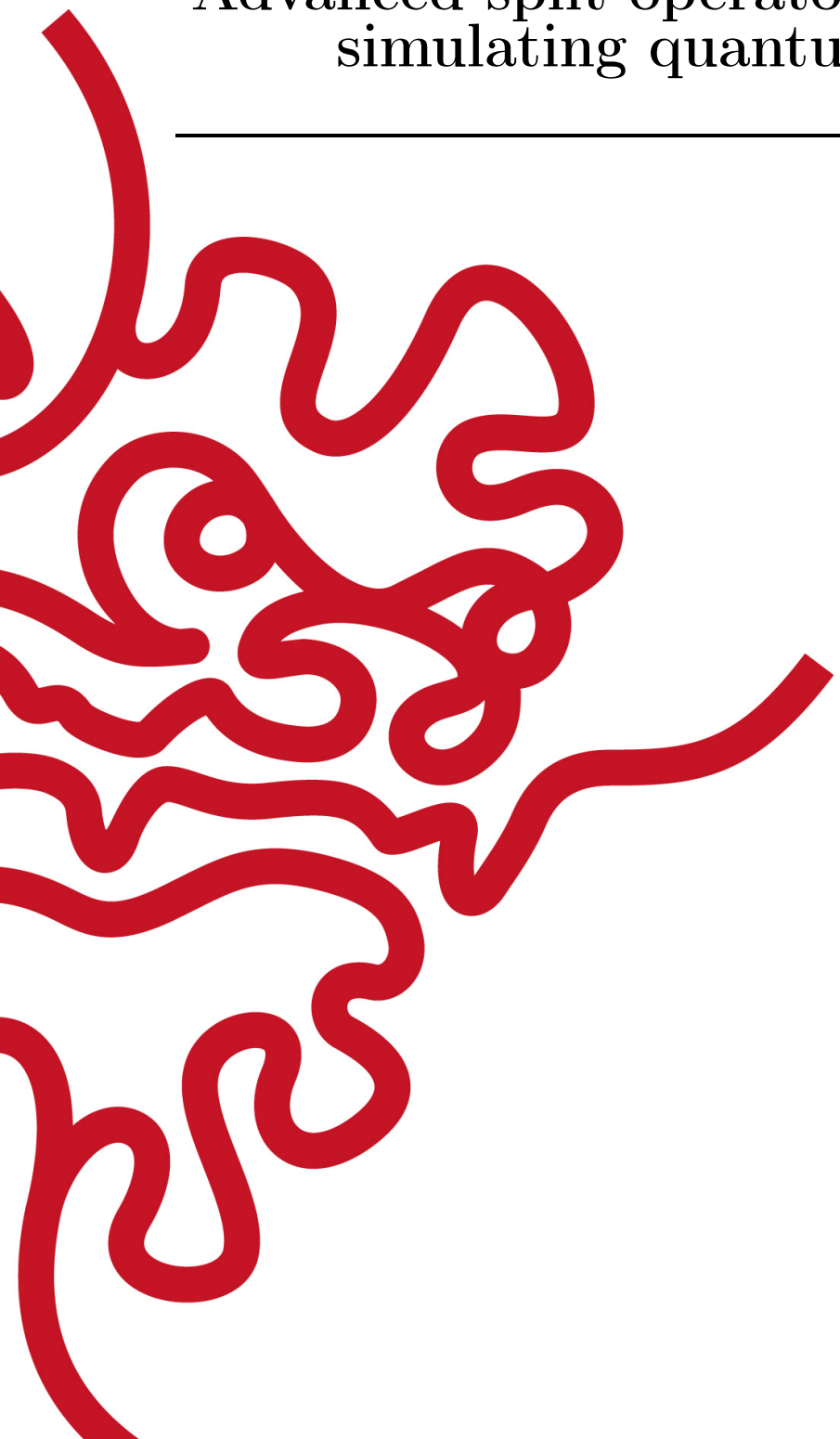

by

James Schloss

Supervisor: **Thomas Busch**

July, 2019

Contents

Chapter 1

Generation, control and detection of 3D vortex structures in superfluid systems

In this chapter, we provide another novel application of the GPUE codebase, this time to the controlled creation of vortex structures in three dimensions with artificial magnetic fields generated by an optical nanofiber. This is the first experimentally realizable device to generate vortex ring-like structures in this manner, and it also provides a method to detect whether a vortex ring is present in an elliptic-toroidal condensate. This project encompasses three-dimensional vortex dynamics and coupled light-matter systems, so to begin, I will discuss the dynamics of vortices in three-dimensional systems, followed by the model used for this project, where I will describe how the light from an optical nanofiber can generate and control vortex structures in BEC systems. This chapter will largely follow the work of Schloss *et. al.* [**?**] [put ArXiv link when available].

1.1 Vortex ring dynamics in BEC systems

As mentioned in Chapter **??**, in BEC systems with large amounts of angular momentum and a single axis of rotation, the vortices will create a triangular, Abrikosov lattice [1, 2]. This regular structure is a direct consequence of the quantization of angular momentum

in quantum mechanics, and in Chapter **??**, I discussed a small vortex lattice in two-dimensions by integrating out the $\hat{z}$ direction. In this chapter, I will discuss the full three-dimensional behavior of vortex structures in BEC systems. In three dimensions, BEC systems have been shown to support a large variety of flow-related excitations, such as vortex lines and rings [1, 3–9]. There are many interesting features to superfluid vortices in three dimensions, many of which follow from classical fluid dynamic theory [10], which is a well-studied field and covered in many texts [11–14]. To start, I will discuss the dynamics of vortex rings in BEC systems.

In a three-dimensional BEC and other superfluid systems, vortices can be described as systems of freely-moving, current-carrying filaments located along the axis of rotation. In this way, it is possible to model such systems using the Biot-Savart law [15]

$$\boldsymbol{v}_s(\boldsymbol{r},t) = \frac{\kappa}{4\pi}\int \frac{|s_1-\boldsymbol{r}|\times ds_1}{|s_1-\boldsymbol{r}|^3}, \tag{1.1}$$

where $\kappa = \hbar/m$ is the circulation. Modelling a superfluid system in this way is the heart of the vortex filament model, and allows us to attain an intuitive understanding for the motion of vortices in a superfluid system; however, it falls short in several areas, such as sound wave propagation and vortex reconnections [16]. Even so, many of the dynamics discussed in this section can be understood with the Biot-Savart law. This model is traditionally taught alongside electrodynamics, where current can only flow within a closed loop or between two conductors. Similarly, when a vortex filament is generated by injecting angular momentum into a superfluid system, it must either end at the edges of the superfluid or reconnect with other vortices.

By modifying our axis of rotation or inducing a vortex structure with either artificial magnetic fields or phase imprinting, we may create three-dimensional topologies, like the vortex ring. This structure is also common in large, three dimensional modelling of superfluid systems and is a direct consequence of the required connections of vortex lines. The stability of vortex rings is ensured by Kelvin's theorem [17], which means that

unstable excitations may decay into vortex rings or objects with ring-like topology [5].

We will begin our discussion of vortex rings with the thin-core approximation in inviscid fluids, as described by Barenghi and Donnelly [18]. If we imagine a thin vortex ring of radius $R \gg a$, where a is the core radius, and with circulation Γ moving in an inviscid fluid with density ρ, the kinetic energy of the ring is given by

$$E = \frac{1}{2}\rho\Gamma^2 R\left[\ln\left(\frac{8R}{a}\right) - \alpha\right], \tag{1.2}$$

where α is a parameter determined by the system, and different values of α correspond to different core models for vortex motion. For example, it is 1.615 for the GPE [19]. The momentum of the system is given by

$$p = \rho\Gamma\pi R^2, \tag{1.3}$$

and the self-induced velocity is [20]

$$v = \frac{\partial E}{\partial p} = \left(\frac{\Gamma}{4\pi R}\left[\ln(\frac{8R}{a}) - \beta\right]\right), \tag{1.4}$$

with $\beta = \alpha - 1$ under constant pressure, and $\beta = \alpha - 3/2$ under constant volume. This method of vortex ring analysis has been extended to rings with finite, but small values for the core radius [21, 22]. These equations come from the Biot-Savart law (Equation (1.1)) above. If we consider a filament that is infinitesimally thin, we find an energy $E = \rho\Gamma^2 R/2$ and a velocity of $v = \Gamma/4\pi R$.

In the case of multiple interacting vortex rings, we can expect to find many similar features in superfluids to what has been found previously in classical, viscous fluids. If two vortex rings are generated in the same plane and in close proximity, it could be possible for the two velocity fields to interact, causing one ring to expand and slow down while the other contracts and speeds up. Under the right conditions, the lagging ring can pass the forward ring through a process known as *leapfrogging* [23, 24].

In addition to leapfrogging, vortex rings can interact through direct collisions [25]. In superfluid ^{4}He, some of the earliest experiments on vortex collisions with vortex rings were performed by Schwarz in 1968 [26]. In the case of a head-on collision, two identical, moving vortex rings will first grow in size before dispersing into a series of smaller vortex rings around their common circumference [27]. These smaller rings are created by vortex reconnections, which can occur any time vortex lines are facing anti-parallel directions and it is energetically favorable to do so.

Finally, we will briefly discuss vortex reconnections, themselves. As predicted by Feynman in 1955, vortex reconnections in a dissipative superfluid systems lead to larger vortices continually reconnecting into smaller ones until the loops become small enough to decay from dissipation or from interactions with boundaries. [28]. These reconnections produce sound waves when vortices directly interact and Kelvin waves when vortices indirectly interact [29]. When a vortex ring structure is not pinned by either gauge fields or rotation, it will evolve naturally by reconnecting into smaller and smaller vortex rings when in a turbulent system [30]. This means that we expect to see vortex reconnections in any sufficiently complicated vortex tangle [31]. In addition, when simulations of vortex rings were performed by Jones and Roberts, they found that by computing vortex rings towards the limit of $R \to a$, they eventually found a solitary wave [32, 33].

Though these dynamics are expected in superfluid systems, it is difficult to devise experimental systems systematically generate the desired behavior. In practice, complex three-dimensional structures cannot be easily created by stirring or rotating a BEC because vortex lines generated in this way must follow the axis of rotation, thus even vortex rings can be a challenge to create, control, and detect experimentally. In most cases, including in most theoretical proposals, vortex ring generation in BEC systems relies on dynamic processes that do not create eigenstates of the system, such as the decay of dark solitons in multicomponent condensates [5] with the snake instability [34], the collision of symmetric defects [35], or direct density engineering [36, 37]. There are other theoretical proposals that consider interfering two BEC systems [30], using Feschbach resonances [38],

or phase imprinting methods [34]. As a note, in inhomogeniously trapped BEC systems, vortex ring structures are known to be unstable, which has led to difficulties in their experimental observation [39]. In addition, imaging techniques employed for BECs are not suited to identify whether three-dimensional vortex structures are present.

To consistently control and generate more complex three-dimensional structures, methods beyond rotation must be used, and there are only a few known experimental systems that can do so [5, 9]. There is also a large amount of interest in generating more complicated vortex structures, such as vortex knots [40–42]. Artificial magnetic fields seem to be a promising method for the generation of complex three-dimensional vortex structures in BEC systems [43], and in this chapter, we will present a method to generate vortex rings, ring-lattices, and other vortex structures in three dimensions by using the artificial magnetic field generated by an optical nanofiber.

1.2 Controlled creation of three-dimensional vortex structures in Bose–Einstein condensates using artificial magnetic fields

One method to create artificial magnetic fields involves the interaction between an atomic system in a dressed state and an electric field that is tuned near an atomic resonance frequency [44]. In practice, this means that we can create a configurable artificial magnetic field with an appropriately tuned electric field that varies strongly over short distances, such as those found in the near-field regime on the surface of a dielectric system when light undergoes total internal reflection [45]. One such system that suits this purpose and can be used to generate vortex ring structures in BEC systems is the optical nanofiber, which has several propagation modes to facilitate the generation of configurable artificial magnetic fields.

Optical nanofiber systems can be created by heating and stretching optical fibers until

their thinnest region is roughly hundreds of nanometers in diameter [46, 47]. At this scale, the wavelength of light is larger than the diameter of the fiber and the strength of the evanescent field is significantly enhanced [48]. The form of the evanescent field varies significantly depending on the optical modes propagating through the nanofiber, and we will show that this can be used to generate interesting and tunable artificial magnetic fields.

Optical nanofibers are already used in many different experiments with ultracold atoms [49–54], and trapping potentials around 200nm from the fiber surface can be created with two differently detuned input fields [55, 56]. Our proposed device will allow for the creation of vortex rings in BEC systems that are trapped toroidally around the nanofiber at roughly the same distance by coupling the BEC to the evanescent field created by different modes propagating through the nanofiber [57]. A schematic of this system is depicted in Figure 1.1

With this same device, it is also possible to detect whether a vortex ring is present in the system by exciting the scissors mode in an elliptic-toroidal trapping geometry [58–60]. This can be done by tilting the trap radially from the center of the torus, which will cause the BEC to oscillate in and out in the new potential, similar to the oscillation shown in Chapter **??** for a simple harmonic oscillator. Without a vortex present, this oscillation possesses a single frequency, whereas in the presence of a vortex ring, it will contain two frequencies that average to the vortex-less oscillation frequency, similar to scissors mode oscillations from frequencies in a two-dimensional, elliptically-trapped BEC [61–63].

1.2.1 Bose–Einstein condensate dynamics in the presence of an optical nanofiber

As discussed in Chapter **??**, in the presence of artificial magnetic fields, the GPE becomes,

$$i\hbar\frac{\partial\Psi}{\partial t} = \left[\frac{(p - m\mathbf{A}(\mathbf{r}))^2}{2m} + V_{\text{trap}}(\mathbf{r}) + g|\Psi|^2\right]\Psi. \tag{1.5}$$

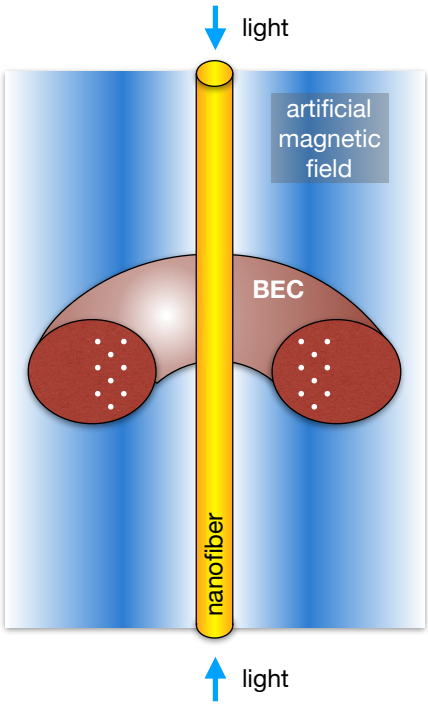

Figure 1.1: Schematic of the system. Blue or red-detuned light is sent into the nanofiber (yellow), creating an evanescent field and artificial magnetic field (blue) that influences the BEC (maroon) held by a toroidal trapping potential. If the artificial magnetic field strength is greater than a threshold value, vortex rings (white) will appear and begin to arrange themselves into a triangular lattice.

Here, all values are defined as before. The artificial vector potential can take many forms, but for these purposes, we will again choose a description based on Berry's connection [44],

$$\mathbf{A} = i\hbar \langle \Psi_l | \nabla \Psi_l \rangle \,, \tag{1.6}$$

where Ψ_l is the atomic wavefunction in some dressed state l.

In this case, we are considering dressed, two-state atoms in the presence of an optical

field and can write these states with the rotating wave approximation as [45],

$$|\Psi_1(\mathbf{r})\rangle = \begin{pmatrix} \cos[\Phi(\mathbf{r})/2] \\ \sin[\Phi(\mathbf{r})/2]e^{i\phi(z)} \end{pmatrix}, \tag{1.7}$$

$$|\Psi_2(\mathbf{r})\rangle = \begin{pmatrix} -\sin[\Phi(\mathbf{r})/2]e^{-i\phi(z)} \\ \cos[\Phi(\mathbf{r})/2] \end{pmatrix}, \tag{1.8}$$

where $\phi(z)$ is the phase of the optical field and $\Phi(\mathbf{r}) = \arctan(|\kappa(\mathbf{r})|/\Delta)$, with $\Delta = \omega_0 - \omega$ being the detuning and $\kappa(\mathbf{r}) = \mathbf{d} \cdot \mathbf{E}(\mathbf{r})/\hbar$ being the Rabi frequency. The atomic dipole moment is given by $\mathbf{d}$ and $\mathbf{E}(\mathbf{r})$ is the electric field. Here we see that the form of $\mathbf{A}$ follows the form of the optical fields, and the artificial magnetic field is given by $\mathbf{B} = \nabla \times \mathbf{A}$; therefore, it is possible to influence the magnetic field and vortex structures generated with this system by modifying the optical profile of the nanofiber.

For optical nanofibers, one can determine which modes will propagate in the system by calculating the V-number, with $V = k_0 a\sqrt{n_1^2 - n_2^2}$, where a is the fiber radius, n_1 is the refractive index of the fiber, n_2 is the refractive index of the cladding, and $k_0 = \omega/c$ with ω being the frequency of the input light beam. In this system, the fiber has been tapered such that the cladding is the vacuum, itself, with $n_2 = 1$. The V-number can be easily controlled by choosing the fiber radius, and higher order modes can only be sustained if $V > V_c \simeq 2.405$. Below this value, only the fundamental mode can propagate in the system.

Using cylindrical coordinates, the evanescent field of the $\mathrm{HE}_{\ell m}$ mode with circular polarization is [64],

$$E_r = iC[(1-s)K_{\ell-1}(qr) + (1+s)K_{\ell+1}(qr)]e^{i(\omega t - \beta z)}, \tag{1.9}$$

$$E_\phi = -C[(1-s)K_{\ell-1}(qr) - (1+s)K_{\ell+1}(qr)]e^{i(\omega t - \beta z)}, \tag{1.10}$$

$$E_z = 2C(q/\beta)K_\ell(qr)e^{i(\omega t - \beta z)}, \tag{1.11}$$

where

$$s = \frac{1/h^2a^2 + 1/q^2a^2}{J'_\ell(ha)/[haJ_\ell(ha)] + K'_\ell(qa)/[qaK_\ell(qa)]}, \tag{1.12}$$

$$C = \frac{\beta}{2q}\frac{J_\ell(ha)/K_\ell(qa)}{\sqrt{2\pi a^2(n_1^2N_1 + n_2^2N_2)}}, \tag{1.13}$$

and

$$\begin{aligned} N_1 =& \frac{\beta^2}{4h^2}\Big[(1-s)^2\left[J_{\ell-1}^2(ha) + J_\ell^2(ha)\right] \\ &+ (1+s)^2\left[J_{\ell+1}^2(ha) - J_\ell(ha)J_{\ell+2}(ha)\right]\Big] \\ &+ \frac{1}{2}\left[J_\ell^2(ha) - J_{\ell-1}(ha)J_{\ell+1}(ha)\right], \end{aligned} \tag{1.14}$$

$$\begin{aligned} N_2 =& \frac{J_\ell^2(ha)}{2K_\ell^2(qa)}\Bigg(\frac{\beta^2}{4q^2}\Big[(1-s)^2\left[K_{\ell-1}^2(qa) - K_\ell^2(qa)\right] \\ &- (1+s)^2\left[K_{\ell+1}^2(qa) - K_\ell(qa)K_{\ell+2}(qa)\right]\Big] \\ &- \frac{1}{2}\left[K_\ell^2(qa) + K_{\ell-1}(qa)K_{\ell+1}(qa)\right]\Bigg). \end{aligned} \tag{1.15}$$

The mode geometry is given by $J_n(x)$, the Bessel function of the first kind, $K_n(x)$, the modified Bessel function of the second kind, and β, the propagation constant of the fiber. The scaling factors are given by $q = \sqrt{\beta^2 - n_2^2k_0^2}$ and $h = \sqrt{n_1^2k_0^2 - \beta^2}$, the normalization constant is C and s is a dimensionless parameter.

When the input light field is linearly polarized, it is convenient to write the Cartesian

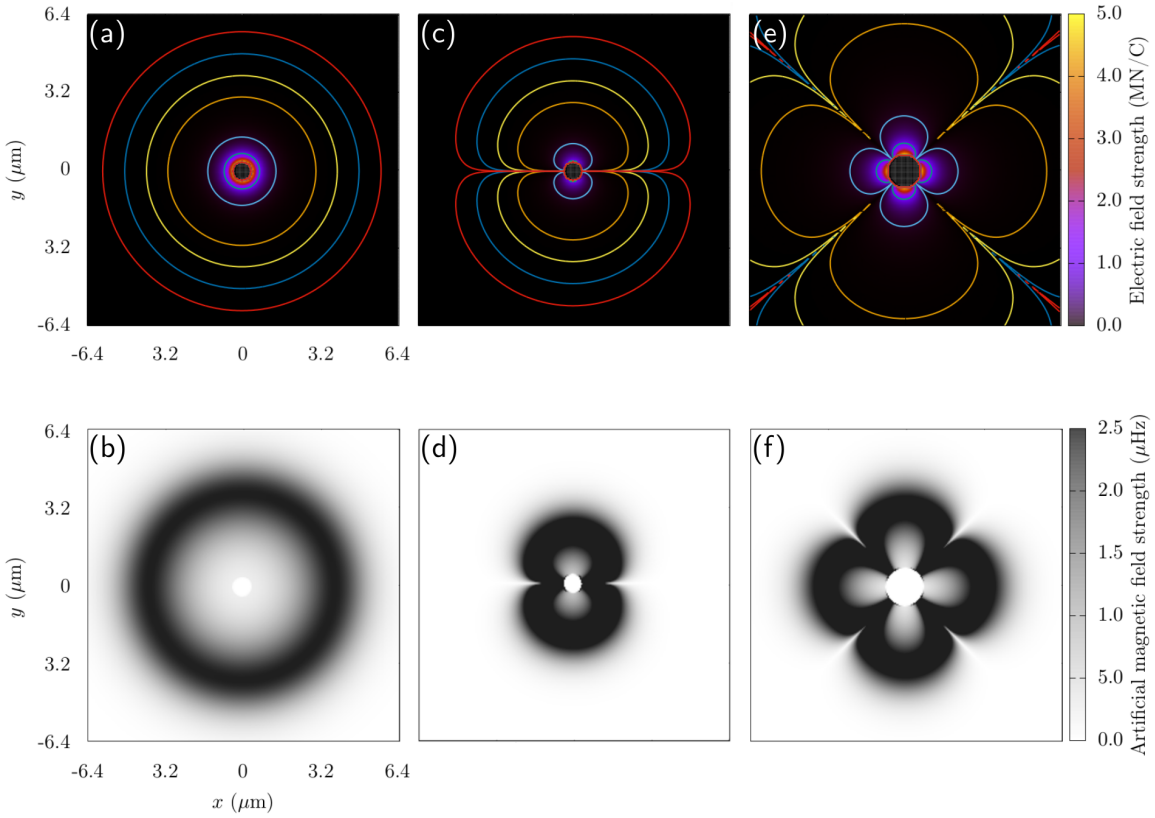

Figure 1.2: Images of electric and artificial magnetic field profiles for [(a) and (b)] the fundamental HE_{11} mode with circular polarization, [(c) and (d)] the HE_{11} mode with linear polarization, and [(e) and (f)] the HE_{21} mode with linear polarization. For these calculations, the input power is 372 nW in (a) and (b) , 16 nW in (c) and (d), and 418 nW in (e) and (f). For the HE_{11} mode, the nanofiber radius is 200 nm with blue-detuned light of 700 nm, and for the HE_{21} mode, the nanofiber radius is 400 nm with red-detuned light of 980 nm

components of the evanescent electric field as

$$E_x = \sqrt{2}C\Big[(1-s)K_{\ell-1}(qr)\cos(\phi_0) + (1+s)K_{\ell+1}(qr)\cos(2\phi-\phi_0)\Big]e^{i(\omega t-\beta z)}, \tag{1.16}$$

$$E_y = \sqrt{2}C\Big[(1-s)K_{\ell-1}(qr)\sin(\phi_0) + (1+s)K_{\ell+1}(qr)\sin(2\phi-\phi_0)\Big]e^{i(\omega t-\beta z)}, \tag{1.17}$$

$$E_z = 2\sqrt{2}iC(q/\beta)K_{\ell}(qr)\cos(\phi-\phi_0)e^{i(\omega t-\beta z)}. \tag{1.18}$$

Here ϕ_0 determines the orientation of polarization, with $\phi_0 = 0$ being along the x axis and $\pi/2$ being along the y axis. The artificial vector potential produced by such evanescent fields around an optical nanofiber is then given by [57]

$$\mathbf{A} = \hat{z}\hbar\kappa_0(n_1+1)\tilde{s}\left[\frac{|d_rE_r + d_\phi E_\phi + d_zE_z|^2}{1+\tilde{s}^2|d_rE_r + d_\phi E_\phi + d_zE_z|^2}\right], \tag{1.19}$$

where $\tilde{s} = \frac{|\mathbf{d}\cdot\mathbf{E}|}{\hbar|\Delta|}$ and the corresponding magnetic field $\mathbf{B} = \nabla \times \mathbf{A}$ can be calculated to be

$$\begin{aligned}\mathbf{B} =& \frac{\hbar\kappa_0 s^2(n_1+1)}{(1+\tilde{s}^2|d_rE_r + d_\phi E_\phi + d_zE_z|^2)^2} \\ &\times \left[\hat{\phi}\frac{\partial}{\partial r}|d_rE_r + d_\phi E_\phi + d_zE_z|^2 \right. \\ &\left. - \hat{r}\frac{1}{r}\frac{\partial}{\partial\phi}|d_rE_r + d_\phi E_\phi + d_zE_z|^2\right].\end{aligned} \tag{1.20}$$

This shows that the $\mathbf{B}$ field has only components in the $\hat{\phi}$ and $\hat{r}$ directions, which means that all field lines lie in the horizontal plane if the fiber is aligned along the vertical $\hat{z}$ direction.

This means that a BEC trapped toroidally around the nanofiber would facilitate vortex structures that wrap around the nanofiber and potentially close on themselves in the form of vortex rings; however, other vortex structures are possible as well. In addition, the value of $\tilde{s}$ governs the amplitude and range of the magnetic field, and as such, it is possible to manipulate the size and shape of the generated vortex rings by changing the detuning and intensity of the electric field [57].

For the purposes of this project, we will consider the fundamental HE_{11} mode with circular polarization, the HE_{11} mode with linear polarization, and the HE_{21} mode with linear polarization. Though even higher-order modes may be generated by the optical nanofiber, increasing the V-number to facilitate these modes also requires increasing the fiber radius outside of what is experimentally achievable considering the toroidally-trapped BEC. It is also possible to create even more complex field configurations by interfering different modes; however, the chosen modes will still demonstrate a range of possible

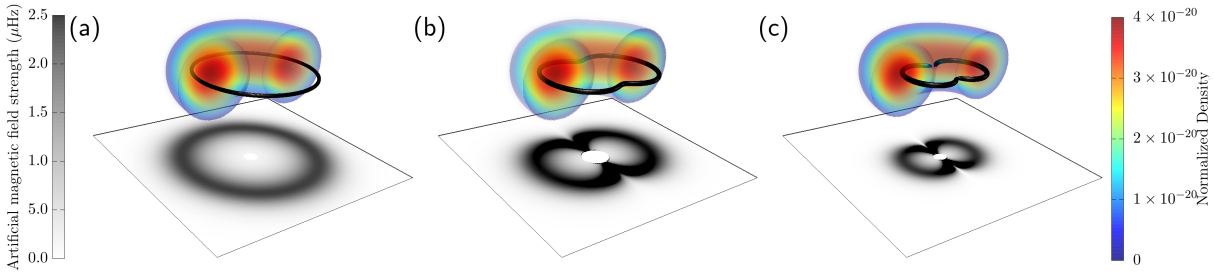

Figure 1.3: Vortex configurations for different magnetic field profiles from the nanofiber for the fundamental HE_{11} mode with (a) circular polarization, (b) elliptical polarization, and (c) linear polarization along the $\hat{y}$ direction. The vortex distributions have been found via an isosurface on the Sobel filtered wavefunction density for a ^{87}Rb BEC and all optical fiber fields are normalized and for a nanofiber of 200 nm in radius with blue-detuned light of 700nm. The magnetic field profiles shown in the shaded region beneath wavefunction density are similar to those in Figure 1.2(b) and (d).

magnetic field profiles. The electric field configurations and their corresponding magnetic field profiles can be seen in Figure 1.2. Here, we see in that the circularly polarized HE_{11} mode will create a cyllindrically symmetric electric (a) and magnetic (b) field profiles; however, linearly polarized light will create a lobed structure for both (c and d). When using the linearly-polarized HE_{21} mode, we see four petals appear in the electric and magnetic field profiles, which suggest unusual vortex structures. Now I will discuss what types of vortex structures can be generated with this system, including the possibility of generating vortex ring lattices.

1.2.2 Possible vortex configurations

For these simulations, we will be using GPUE [65] to describe a ^{87}Rb condensate with 1×10^5 atoms with a scattering length of $a_s = 4.76 \times 10^{-9}$ m on a three-dimensional grid of 256^3 points with a spatial resolution of 50 nm, and we assume a toroidal trapping potential around the fiber given by,

$$V_{\text{trap}} = m(\omega_r^2(r-\eta)^2 + \omega_z^2 z^2), \tag{1.21}$$

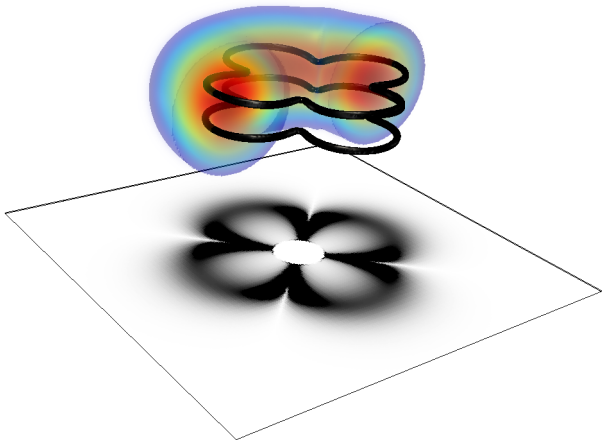

Figure 1.4: Vortex configuration for the HE_{21} mode with linear polarization along the $\hat{y}$ direction. The magnetic field profile is similar to the one shown in Figure 1.2(f), and has been calculated for a nanofiber of 400 nm in radius with red-detuned light of 980 nm.

where we choose the frequencies in the $\hat{r}$ and $\hat{z}$ directions to be $\omega_r = \omega_z = 7071$Hz to match typical experimental conditions in fiber trapping [49]. Here, η describes the distance of the center of the torus from the center of the fiber and is chosen such that the atoms are trapped beyond the van-der-Waals potential of the fiber. For the HE_{11} mode, the fiber radius is 200 nm and $\eta = 3.20\,\mu$m, creating a toroidal BEC with an inner radius of roughly 300 nm from the fiber surface. For the HE_{21} mode, we increase the fiber radius to 400 nm, but keep all other parameters the same, creating a toroidal BEC with an inner radius of roughly 150 nm.

As shown in Figure 1.3(a), when simulating the HE_{11} mode with these parameters, we see a vortex line that wraps around the fiber and reconnect in the form of a single vortex ring as the ground state solution. In contrast, the linearly polarized HE_{11} mode in Figure 1.3(c) shows a ground state where the vortex lines bend toward the center of the torus, creating two vortex lobes. As a note, the vortex lines do not follow the magnetic field lines exactly, but instead reconnect to the neighboring lobe when approaching each other within a healing length. If elliptically polarized light is considered, we see a hybrid ground state between the circularly and linearly polarized modes, shown in Figure 1.3(b). Finally, we show a four-petal ground-state solution when using the HE_{21} linearly polarized

mode in Figure 1.4. Here, we also show that it is possible to generate multiple vortex structures in-line with themselves by increasing the intensity of the artificial magnetic field.

This indicates that it is possible to generate interesting vortex ring lattice structures in three-dimensions by sufficiently increasing the artificial magnetic field. To study the control of multiple vortex structures with this system, we first simulated a system with low artificial magnetic field strength and showed that this simulation will cause all vortex rings to line up at peaks in the magnetic field in Figure 1.5(a and b). As the magnetic field is increased from this point, we see that the vortex rings begin to pack together and form an Abrikosov-like lattice in-line with peaks in the artificial magnetic field, shown in Figure 1.5(a and c). If other magnetic field profiles are used, it could be possible to generate different Abrikosov-like ring lattice configurations. This system could allow for studies of bulk vortex-ring movement, thereby potentially creating a vortex ring lattice that rotates in a leapfrogging manner and moves based on individual vortices self-induced velocity.

The optical nanofiber seems to provide unprecedented control over the vortex geometries generated in a toroidally-trapped BEC system, and one can control the shape of each vortex structure by manipulating the optical fields input into the nanofiber. In addition, because the optical fields could be time-dependent, this system could be used in the future to probe dynamical effects of vortices. In this case, one must consider the effects of high artificial magnetic fields on the distribution of atoms, themselves, because (as described in Chapter **??**), the external potential V_{trap} will be modified by a term proportional to $\mathbf{A}^2$. In Figure 1.6, we show this modification for the artificial magnetic fields shown in Figure 1.5(c). Dynamical studies here will thus lead to phonon excitations in the condensate, which will also influence the vortices, themselves, and this is an area of future work.

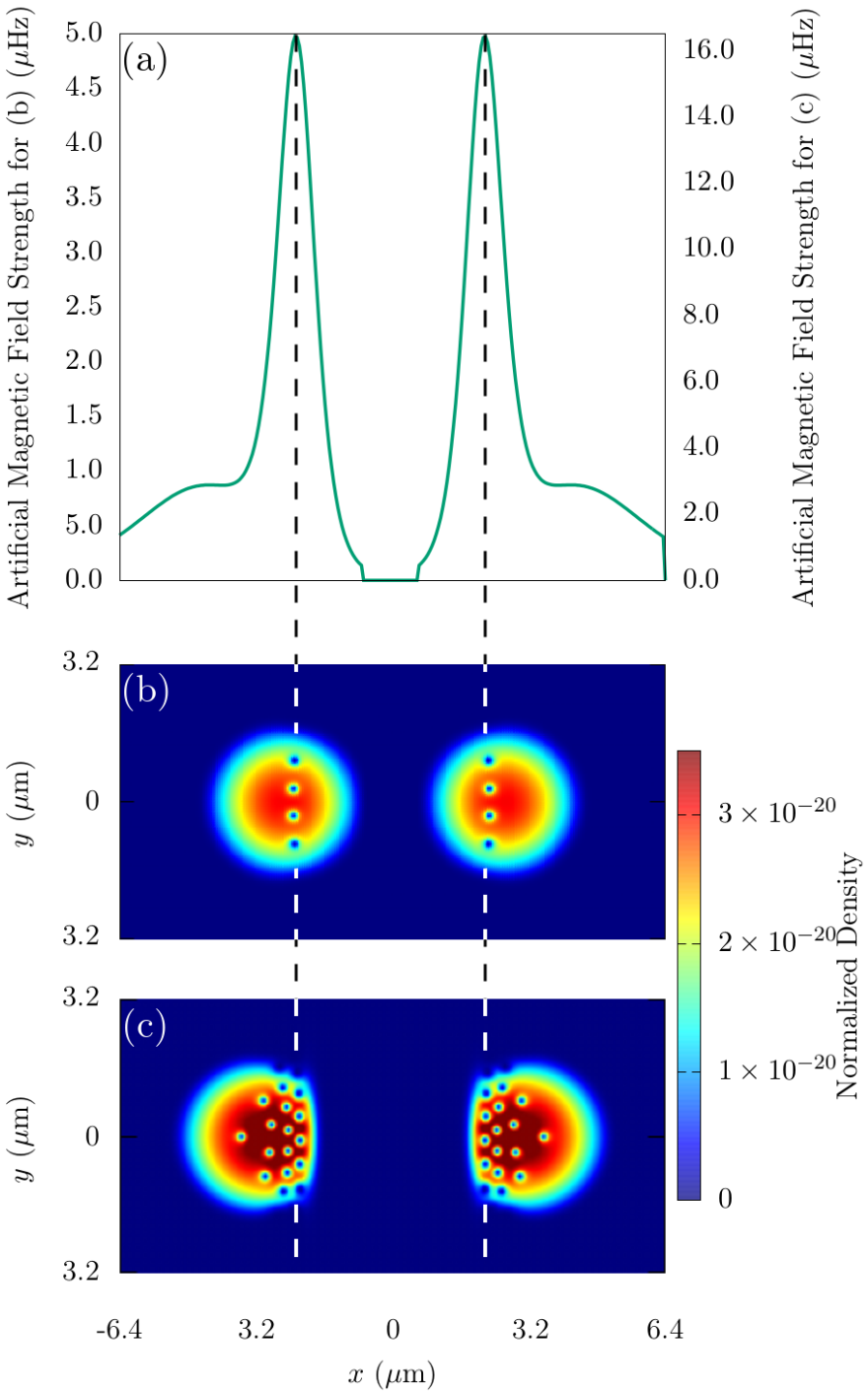

Figure 1.5: (a) The magnetic field profile along the x-direction for the fundamental HE_{11} mode with circular polarization outside a fiber of 200 nm radius. Note that for this mode and polarization the whole system is azimuthally symmetric. For weak fields (see (b)) this leads to a small number of vortices that align along the line at which the magnetic field is maximal and for larger fields (see (c)) more vortex rings appear that form the beginning of an Abrikosov lattice. The optical fiber field and wavefunction density have been normalized and are for a nanofiber of 200 nm in diameter with blue-detuned light of 700nm and a ^{87}Rb BEC respectively.

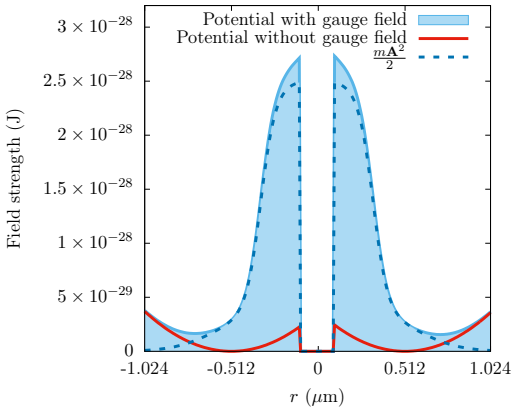

Figure 1.6: Visualization of the change in potential due to the effects of the artificial magnetic field for Figure 1.5. Here, the experienced potential is shown in the blue shaded region, the scaled artificial vector potential is shown as a dotted, dark blue line, and the original trap is shown in red.

1.2.3 Dynamic vortex detection and scissor modes

Observing the presence of vortex rings in a three dimensional BEC is a difficult problem, as absorption spectroscopy usually only provides a picture of an integrated two-dimensional density. However, due to the unique geometry of this system, we can identify whether vortex rings are present by exciting the scissors mode of the condensate [58–60]. For an elliptic-toroidal geometry ($\omega_z < \omega_r$), the scissors mode can be excited by modifying the external potential with a rotation in the rz-plane,

$$V = V_{\text{trap}}(r, \theta, z) - m\omega_0^2 \alpha r z, \tag{1.22}$$

where $\alpha = 2\epsilon\theta$ is a coefficient related to the tilting angle, ϵ is the deformation of the trap in the rz plane and θ is the angle at which the original trap was aligned at. For a small initial angle of θ_0 this change in the potential causes a BEC without rotation to oscillate back and forth in the trap with a frequency given by [63]

$$\omega_{\text{scissors}} = \sqrt{\omega_r^2 + \omega_z^2}. \tag{1.23}$$

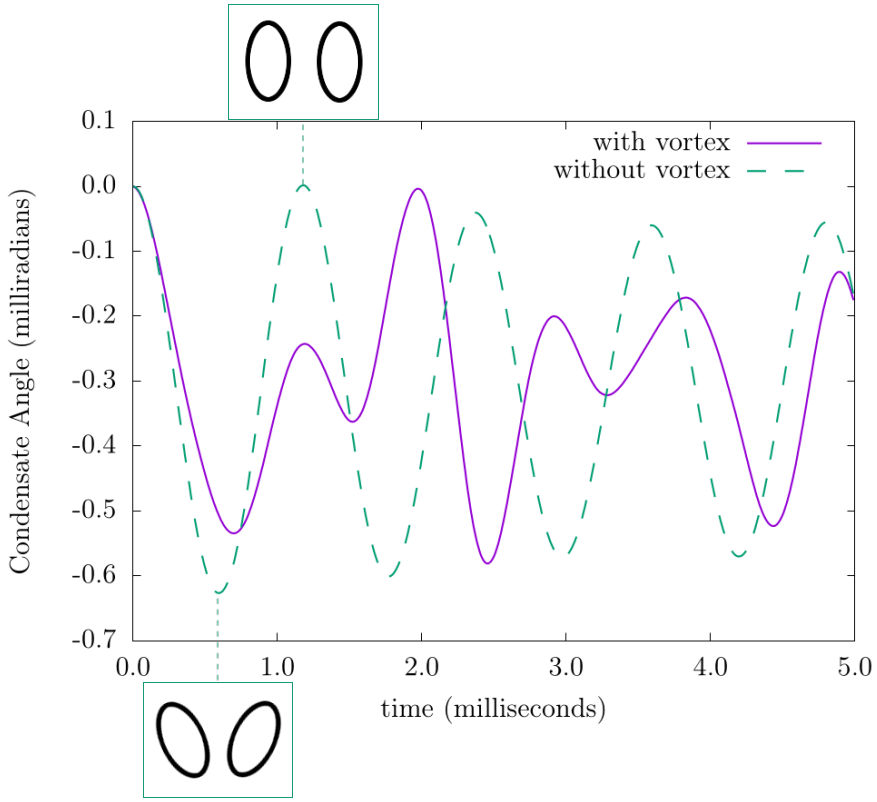

Figure 1.7: Angle of the condensate axis after excitation of the toroidal scissors mode for an elliptic-toroidal BEC with a single vortex ring (purple, solid) and without a vortex present (cyan, dashed). Depictions of two dimensional slices for the scissors mode without a vortex are shown in the insets. Here we see that the scissors mode causes oscillation in and out towards the center of the system, and that two distinct frequencies are present in the curve for the condensate carrying a vortex ring.

If, however, this mode is excited for a BEC that contains a vortex line, the oscillation will be strongly influenced by the currents inside the condensate and two different frequencies (ω_+ and ω_-) appear in the oscillation [61–63]. When the splitting frequency is small compared to the scissors mode frequency, it can be written as [62]

$$\omega_+ - \omega_- = \frac{\langle l_z \rangle}{m\langle r^2 + z^2 \rangle}, \tag{1.24}$$

where $\langle l_z \rangle$ is the average angular momentum per particle. Calculating these values for our system for $\omega_r = 4242$Hz, and $\omega_z = 2828$Hz then leads to $\omega_{\text{scissors}} = 5090$Hz, $\omega_- = 3765$Hz, and $\omega_+ = 6415$Hz, which are very close to the values observed in the numerical simulations shown in Fig. 1.7. However, one can also see from this figure that the oscillation is not perfect and seems to decay over time. This is due to the above mentioned modification of the trapping potential by the artificial vector potential, which leads to a deviation from the perfect elliptical toroidal shape used in the derivation of Equation (1.24).

It is worth noting that this method cannot be used to detect a vortex ring inside a simply connected condensate, as in this situation the flow around the vortex line has no preferred direction. However, in the toroidal shape, each radial slice can be seen as a two-dimensional elliptical BEC with a single vortex, and the system will therefore exhibit the scissors mode frequency as expected. While in principle the excitation of the scissors mode can also be used to detect Abrikosov vortex-ring lattice, the fact that the inhomogeneous artificial magnetic field leads to an inhomogeneous vortex ring distribution will have an effect on the expected oscillation frequencies.

1.3 Conclusion

In this application of the GPUE codebase, we have shown that it is possible to create and control vortex rings and more complicated vortex structures by using the artificial magnetic field generated by the optical nanofiber. There is currently no other known

method to generate the structures created by the linearly polarized modes, shown in Figure 1.3(b,c) and 1.4. We have also shown that the scissors mode can be used to detect whether a vortex ring is present in an elliptic toroidal trap. These fiber-generated structures could allow for experimental systems to study complicated superfluid mechanisms, like the kelvin-mode cascade, superfluid turbulence, or reconnection events between superfluid vortex lines. These structures might also be the first step in creating knotted vortex lines around an optical nanofiber; however, to generate these structures, the magnetic field must have a dependence on $\hat{z}$, which is not present in this model.

This project leaves several open fields of study for future work and future simulations with GPUE, including the study of dynamic field effects on vortex structures, the generation of vortex knots in superfluid systems with this device, and studies of vortex ring lattice movement in BEC systems. For both of these cases, significant work must be performed both theoretically and computationally.

Bibliography

[1] JR Abo-Shaeer, C Raman, JM Vogels, and Wolfgang Ketterle. Observation of vortex lattices in bose-einstein condensates. *Science*, 292(5516):476–479, 2001.

[2] AA Abrikosov. The magnetic properties of superconducting alloys. *Journal of Physics and Chemistry of Solids*, 2(3):199–208, 1957.

[3] KW Madison, F Chevy, W Wohlleben, and Jl Dalibard. Vortex formation in a stirred bose-einstein condensate. *Physical review letters*, 84(5):806, 2000.

[4] Daniel H Wacks, Andrew W Baggaley, and Carlo F Barenghi. Large-scale superfluid vortex rings at nonzero temperatures. *Physical Review B*, 90(22):224514, 2014.

[5] B. P. Anderson, P. C. Haljan, C. A. Regal, D. L. Feder, L. A. Collins, C. W. Clark, and E. A. Cornell. Watching dark solitons decay into vortex rings in a bose-einstein condensate. *Phys. Rev. Lett.*, 86:2926–2929, Apr 2001.

[6] Aurel Bulgac, Michael McNeil Forbes, Michelle M Kelley, Kenneth J Roche, and Gabriel Wlazłowski. Quantized superfluid vortex rings in the unitary fermi gas. *Physical review letters*, 112(2):025301, 2014.

[7] Mark JH Ku, Biswaroop Mukherjee, Tarik Yefsah, and Martin W Zwierlein. Cascade of solitonic excitations in a superfluid fermi gas: From planar solitons to vortex rings and lines. *Physical review letters*, 116(4):045304, 2016.

[8] Michael Robin Matthews, Brian P Anderson, PC Haljan, DS Hall, CE Wieman, and

Eric A Cornell. Vortices in a bose-einstein condensate. *Physical Review Letters*, 83(13):2498, 1999.

[9] Tarik Yefsah, Ariel T Sommer, Mark JH Ku, Lawrence W Cheuk, Wenjie Ji, Waseem S Bakr, and Martin W Zwierlein. Heavy solitons in a fermionic superfluid. *Nature*, 499(7459):426, 2013.

[10] Alexander L. Fetter. Rotating trapped bose-einstein condensates. *Rev. Mod. Phys.*, 81:647–691, May 2009.

[11] T. E. Faber. *Fluid Dynamics for Physicists*. Cambridge University Press, 1995.

[12] Ira M. Cohen David R. Dowling, Pijush K. Kundu. *Fluid Mechanics*. Academic Press, Boston, fifth edition edition, 2012.

[13] D. J. Tritton. *Physical Fluid Dynamics*. Oxford University Press, 1988.

[14] L. D. Landau and E. M. Lifshitz. *Fluid Mechanics*. Butterworth-Heinemann, 1987.

[15] K. W. Schwarz. Three-dimensional vortex dynamics in superfluid ^{4}He: Line-line and line-boundary interactions. *Phys. Rev. B*, 31:5782–5804, May 1985.

[16] S. Zuccher, M. Caliari, A. W. Baggaley, and C. F. Barenghi. Quantum vortex reconnections. *Physics of Fluids*, 24(12), 2012.

[17] R. Donnelly. *Quantized Vortices in Helium II*. Cambridge University Press, 1991.

[18] C F Barenghi and R J Donnelly. Vortex rings in classical and quantum systems. *Fluid Dynamics Research*, 41(5):051401, 2009.

[19] P. H. Roberts and J. Grant. Motions in a bose condensate. I: The structure of a large circular vortex. *J. Phys.*, 4:55, 1971.

[20] P. H. Roberts and R. J. Donnelly. Dynamics of vortex rings. *Phys. Lett.*, 31A:137, 1970.

[21] L. E. Fraenkel. On steady vortex rings of small cross-section in an ideal fluid. *Proceedings of the Royal Society of London A: Mathematical , Physical and Engineering Sciences*, 316(1524):29–62, 1970.

[22] L. E. Fraenkel. Examples of steady vortex rings of small cross-section in an ideal fluid. *Journal of Fluid Mechanics*, 51:119–135, 1 1972.

[23] A. Sommerfield. *Mechanics of Deformable Bodies: Lectures of Theoretical Physics*, volume 2. Academic Press, 1960.

[24] R. M. Caplan, J. D. Talley, and P. G. Carretero-González, R. a nd Kevrekidis. Scattering and leapfrogging of vortex rings in a superfluid. *Physics of Fluids*, 26(9), 2014.

[25] K Shariff and A Leonard. Vortex rings. *Annual Review of Fluid Mechanics*, 24(1):235–279, 1992.

[26] K. W. Schwarz. Interaction of quantized vortex rings with quantized vortex lines in rotating he II. *Phys. Rev.*, 165:323–334, Jan 1968.

[27] T. T. Lim and T. B. Nickels. *Fluid Vortices*. Springer Netherlands, Dordrecht, 1995.

[28] R. P. Feynman. *Progress in Low Temperature Physics: Chapter II, Application of Quantum Mechanics to Liquid Helium*, volume 1. Interscience Publishers Inc, 1955.

[29] Matthew S. Paoletti and Daniel P. Lathrop. Quantum turbulence. *Annual Review of Condensed Matter Physics*, 2(1):213–234, 2011.

[30] B. Jackson, J. F. McCann, and C. S. Adams. Vortex line and ring dynamics in trapped Bose–Einstein condensates. *Phys. Rev. A*, 61:013604, Dec 1999.

[31] Carlo F. Barenghi, Ladislav Skrbek, and Katepalli R. Sreenivasan. Introduction to quantum turbulence. *PNAS*, 111:4647, 2014.

[32] C A Jones and P H Roberts. Motions in a bose condensate. iv. axisymmetric solitary waves. *Journal of Physics A: Mathematical and General*, 15(8):2599, 1982.

[33] Natalia G. Berloff. Solitary waves on vortex lines in ginzburg-landau models for the example of bose-einstein condensates. *Phys. Rev. Lett.*, 94:010403, Jan 2005.

[34] J. Ruostekoski and J. R. Anglin. Creating vortex rings and three-dimensional skyrmions in Bose–Einstein condensates. *Phys. Rev. Lett.*, 86:3934–3937, Apr 2001.

[35] Naomi S Ginsberg, Joachim Brand, and Lene Vestergaard Hau. Observation of hybrid soliton vortex-ring structures in bose-einstein condensates. *Physical review letters*, 94(4):040403, 2005.

[36] I Shomroni, E Lahoud, S Levy, and J Steinhauer. Evidence for an oscillating soliton/vortex ring by density engineering of a bose–einstein condensate. *Nature Physics*, 5(3):193, 2009.

[37] Janne Ruostekoski and Zachary Dutton. Engineering vortex rings and systems for controlled studies of vortex interactions in bose-einstein condensates. *Physical Review A*, 72(6):063626, 2005.

[38] Florian Pinsker, Natalia G Berloff, and Víctor M Pérez-García. Nonlinear quantum piston for the controlled generation of vortex rings and soliton trains. *Physical Review A*, 87(5):053624, 2013.

[39] M. Abad, M. Guilleumas, R. Mayol, and M. Pi. Vortex rings in toroidal Bose–Einstein condensates. *Laser Physics*, 18(5):648–652, 2008.

[40] F Maucher, SA Gardiner, and IG Hughes. Excitation of knotted vortex lines in matter waves. *New Journal of Physics*, 18(6):063016, 2016.

[41] Dustin Kleckner, Louis H Kauffman, and William TM Irvine. How superfluid vortex knots untie. *Nature Physics*, 12(7):650, 2016.

[42] Renzo L Ricca, David C Samuels, and Carlo F Barenghi. Evolution of vortex knots. *Journal of Fluid Mechanics*, 391:29–44, 1999.

[43] Callum W Duncan, Calum Ross, Niclas Westerberg, Manuel Valiente, Bernd J Schroers, and Patrik Öhberg. Linked and knotted synthetic magnetic fields. *Physical Review A*, 99(6):063613, 2019.

[44] J Dalibard and F Gerbier. Juzeliunas, and p. öhberg. *Rev. Mod. Phys*, 83:1523, 2011.

[45] M. Mochol and K. Sacha. Artificial magnetic field induced by an evanescent wave. *Scientific Reports*, 5, Jan 2015. Article.

[46] Jonathan M Ward, Danny G O'Shea, Brian J Shortt, Michael J Morrissey, Kieran Deasy, and Síle G Nic Chormaic. Heat-and-pull rig for fiber taper fabrication. *Review of scientific instruments*, 77(8):083105, 2006.

[47] Limin Tong, Rafael R Gattass, Jonathan B Ashcom, Sailing He, Jingyi Lou, Mengyan Shen, Iva Maxwell, and Eric Mazur. Subwavelength-diameter silica wires for low-loss optical wave guiding. *Nature*, 426(6968):816, 2003.

[48] Amnon Yariv et al. *Optical electronics in modern communications*, volume 1. Oxford University Press, USA, 1997.

[49] E Vetsch, D Reitz, G Sagué, R Schmidt, ST Dawkins, and A Rauschenbeutel. Optical interface created by laser-cooled atoms trapped in the evanescent field surrounding an optical nanofiber. *Physical review letters*, 104(20):203603, 2010.

[50] C Lacroûte, KS Choi, A Goban, DJ Alton, D Ding, NP Stern, and HJ Kimble. A state-insensitive, compensated nanofiber trap. *New Journal of Physics*, 14(2):023056, 2012.

[51] Thomas Nieddu, Vandna Gokhroo, and Síle Nic Chormaic. Optical nanofibres and neutral atoms. *Journal of Optics*, 18(5):053001, 2016.

[52] G Sagué, E Vetsch, W Alt, D Meschede, and A Rauschenbeutel. Cold-atom physics using ultrathin optical fibers: Light-induced dipole forces and surface interactions. *Physical review letters*, 99(16):163602, 2007.

[53] Laura Russell, Kieran Deasy, Mark J Daly, Michael J Morrissey, and Síle Nic Chormaic. Sub-doppler temperature measurements of laser-cooled atoms using optical nanofibres. *Measurement Science and Technology*, 23(1):015201, 2011.

[54] Ravi Kumar, Vandna Gokhroo, Kieran Deasy, Aili Maimaiti, Mary C Frawley, Ciarán Phelan, and Síle Nic Chormaic. Interaction of laser-cooled 87rb atoms with higher order modes of an optical nanofibre. *New Journal of Physics*, 17(1):013026, 2015.

[55] Fam Le Kien, V. I. Balykin, and K. Hakuta. Atom trap and waveguide using a two-color evanescent light field around a subwavelength-diameter optical fiber. *Phys. Rev. A*, 70:063403, Dec 2004.

[56] C.F. Phelan, T. Hennessy, and Th. Busch. Shaping the evanescent field of optical nanofibers for cold atom trapping. *Opt. Express*, 21(22):27093–27101, Nov 2013.

[57] Rashi Sachdeva and Thomas Busch. Creating superfluid vortex rings in artificial magnetic fields. *Physical Review A*, 95(3):033615, 2017.

[58] Marco Cozzini, Sandro Stringari, Vincent Bretin, Peter Rosenbusch, and Jean Dalibard. Scissors mode of a rotating bose-einstein condensate. *Physical Review A*, 67(2):021602, 2003.

[59] D Guéry-Odelin and S Stringari. Scissors mode and superfluidity of a trapped bose-einstein condensed gas. *Physical review letters*, 83(22):4452, 1999.

[60] OM Marago, SA Hopkins, J Arlt, E Hodby, G Hechenblaikner, and CJ Foot. Observation of the scissors mode and evidence for superfluidity of a trapped bose-einstein condensed gas. *Physical review letters*, 84(10):2056, 2000.

[61] NL Smith, WH Heathcote, JM Krueger, and CJ Foot. Experimental observation of the tilting mode of an array of vortices in a dilute bose-einstein condensate. *Physical review letters*, 93(8):080406, 2004.

[62] Francesca Zambelli and Sandro Stringari. Quantized vortices and collective oscillations of a trapped bose-einstein condensate. *Physical review letters*, 81(9):1754, 1998.

[63] S Stringari. Superfluid gyroscope with cold atomic gases. *Physical review letters*, 86(21):4725, 2001.

[64] Vladimir Georgievich Minogin and Síle Nic Chormaic. Manifestation of the van der waals surface interaction in the spontaneous emission of atoms into an optical nanofiber. *Laser Physics*, 20(1):32–37, 2010.

[65] James R Schloss and Lee J Riordan. Gpue: Graphics processing unit gross-pitaevskii equation solver. *J. Open Source Software*, 3(32):1037, 2018.